International Forum on Aeroelasticity and Structural Dynamics
IFASD 2017
25-28 June 2017 Como, Italy

INFLUENCE OF REDUCED FREQUENCY ON CHOKE FLUTTER INSTABILITY IN TRANSONIC UHBR FAN

Q. Rendu[1], **S. Aubert**[1], **P. Ferrand**[1]

[1]Université de Lyon
ECL, LMFA UMR CNRS 5509
36 av. Guy de Collongue, 69134 Ecully, France
quentin.rendu@gmail.com

Keywords: aeroelasticity, flutter, turbomachinery, linear method, LRANS, acoustic blocage, shock-wave / boundary layer interaction

Abstract: Choke flutter appears when a strong shock-wave chokes the blade to blade channel. The blades vibration lead to the oscillation of the shock-wave. This induces a dynamic loading of the structure which can lead to an aeroelastic instability. In the present work, the physical mechanisms leading to the instability (flutter) are identified through 2D linear RANS aeroelastic computations. A linear decomposition shows that the vibration of the blades downstream of the shock-wave generates a backward travelling pressure wave driving the aeroelastic stability. A local analysis of the downstream vibration demonstrates the destabilising contribution of the shock-wave / separated boundary layer interaction. The source of flutter is finally a combination of inviscid (acoustic blocage) and viscous (unsteady separation) mechanisms.

1 INTRODUCTION

Choke flutter is a critical aeroelastic instability which can lead to the failure of the fan or compressor blades in turbojet engines. In Ultra High Bypass Ratio (UHBR) fan, this instability appears at part speed regimes (typically 80Nn) and at low incidence (high massflow, low total pressure ratio). The steady flow is subsonic upstream of the blade row and supersonic in the blade to blade channel. A strong shock-wave chokes the channel and interacts with the boundary layer on both the suction side and the pressure side. If strong enough, this shock-wave / boundary layer interaction (SWBLI) can lead to the separation of the flow. As the blades vibrate, the shock-wave oscillates and induces a stabilising or destabilising dynamic loading on the structure. The shock-wave motion is known to highly contribute to the aeroelastic behaviour of the blade [1]. Nevertheless, the physical mechanisms leading to choke flutter are not yet understood [2]. Several experimental studies have shown the influence of some parameters (incidence, solidity, ...) on choke flutter margin [3]. However, the local analysis of the unsteady flow is mandatory to understand the underlying mechanisms. Computational Fluid Dynamics (CFD) is usually the only affordable way to obtain a time and space resolved flow field. Regarding the quality of the flow modelling, Petrie-Repar et al. [5] showed that viscous effects are important in off-design operating points (near stall and choke line).

In turbomachinery computational aeroelasticity, the blade stability is generally obtained through the energetic method [4]. This method relies on the radial decomposition of the 3D blade in a sum of 2D airfoils. The damping coefficient is computed on each 2D airfoil and the overall damping coefficient is obtained by an integral along the radius, from hub to tip. It is widely

known, because the velocity and pressure fluctuations are the largest, that the region close to the tip gives the main contribution to the global damping coefficient. In the present study the computational efforts are thus focused on a 2D blade to blade channel extracted at 90% height.

From given fan geometry, operating point and modeshape, a parametric study is run on the interblade phase angle and the reduced frequency to identify unstable configurations. An innovative numerical methodology is then presented to investigate independently the contributions of different zones of the airfoil to the aeroelastic behaviour of the blade. This method relies on the time-linearisation of Reynolds-Averaged Navier-Stokes (RANS) equations.

In the first part, the numerical methods are presented. The airfoils, the steady flow and the modeshape chosen for the aeroelastic study are presented. The aeroelastic behavior of the blade is discussed in the last part thanks to a parametric study and an innovative methodology to identify the mechanisms responsible for choke flutter.

2 NUMERICAL METHODS

2.1 Nonlinear RANS solver

The compressible RANS solver Turb'Flow is used in this work to compute the 2D steady flow in a 90% height blade to blade channel. This solver relies on vertex centred finite volume method on multi-block structured grids [6].

Convective fluxes are obtained through upwind scheme of Roe [7] with Monotonic Upstream-centred Scheme for Conservative Laws (MUSCL) interpolation of third order [8]. The interpolation order is reduced in strong gradient zones according to Harmonic Cubic Upwind Interpolation (H-CUI) limiter. Diffusive fluxes are obtained through central interpolation of conservative variables.

The pseudo time discretisation relies on backward Euler with CFL=20 and local time step to speed up the convergence. The linear problem arising from the implicit method is solved through GMRES iterative method [9].

The flow is considered fully turbulent and the k-ω turbulence model of Wilcox [10] has been used.

2.2 Linear RANS solver

The Linearised RANS (LRANS) solver Turb'Lin is used to compute the harmonic flow around the steady state. This solver has been previously validated on transonic separated flows [11, 12]. The solution is obtained in the frequency domain by solving the linear system. Spatial discretisation relies on Jameson et al. [13] centred scheme with linearised pressure sensor. As the frozen turbulence assumption is not valid for separated flows [11, 12], the turbulence model has also been linearised.

2.3 Aeroelasticity

The complex amplitude of displacement $\widetilde{\delta\mathbf{x}}$ and velocity $\widetilde{\mathbf{V}}$ is imposed at each node of the blade mesh to model the blades oscillation. The steady position of the blade is chosen as the phase origin. This yields

$$\Re(\widetilde{\delta\mathbf{x}}) = 0 \quad ; \quad \Im(\widetilde{\mathbf{V}}) = 0 \tag{1}$$

The interblade phase angle (IBPA) σ is modelled through quasi-periodic boundary conditions in azimuthal direction

$$\widetilde{\boldsymbol{q}}(\boldsymbol{x_b} + \boldsymbol{g}) = \widetilde{\boldsymbol{q}}(\boldsymbol{x_b})\boldsymbol{e^{j\sigma}} \tag{2}$$

where $\widetilde{q}$ is the complex amplitude of conservative variable fluctuations, x_b the domain boundary and g the interblade pitch.

The work $\mathcal{W}$ extracted by the flow to the structure is written according to the convention of Verdon [14]. The damping coefficient is then obtained by the integral of the extracted work along the blade surface

$$\zeta = \frac{1}{4\pi}\frac{\iint_\Omega \mathcal{W}\mathrm{d}\Omega}{\mathcal{U}} \tag{3}$$

where Ω is the fluid-structure contact interface and $\mathcal{U}$ the maximal vibrating kinetic energy. The work can be written as

$$\mathcal{W} = \int_0^T \left[-\widetilde{Ps}(\mathbf{x},t) * \mathbf{S}(\mathbf{x},t)\right]^t \cdot \widetilde{\mathbf{V}}(\mathbf{x},t)\mathrm{d}t \tag{4}$$

where $\widetilde{Ps}$ is the instantaneous static pressure, $\mathbf{S}$ the vector associated to the instantaneous surface, oriented towards the structure, and $\widetilde{\mathbf{V}}$ the instantaneous velocity vector associated to the blade displacement. In frequency domain, neglecting second order terms, the only contribution to the unsteady work is, for a rigid body motion,

$$\Re(\,{}^1\widetilde{Ps})\;\mathbf{S}\cdot\Re(\,{}^1\widetilde{\mathbf{V}}) \tag{5}$$

where ${}^1\widetilde{Ps}$ and ${}^1\widetilde{\mathbf{V}}$ are the complex amplitude of first harmonic of static pressure and velocity vector, respectively. Thus only the real part of fluctuating static pressure contributes to the stability of the fluid-structure interaction.

In next section, the geometry is presented as well as the steady flow and the modeshape chosen for the aeroelastic study.

3 STUDIED CONFIGURATION

3.1 ECL5v1 UHBR fan

The aeroelatic behaviour of the transonic UHBR fan ECL5v1 is studied in this work. This configuration is the first design of ECL5, a 1/4 scaled model representative of UHBR future fans and dedicated to the experimental investigation of aeroelastic and aerodynamic instabilities. The operating range of ECL5v1 is plotted in Figure 1 for three different rotational speeds (nominal speed Nn=10450rpm). The maximum isentropic efficiency, not shown here, varies between 90% and 95% depending on the rotational speed [15].

As already stated, the extracted work depends on both structure velocity and pressure fluctuations. These two parameters are maximum close to the tip. A 2D blade to blade channel mesh has thus been extracted at 90% of ECL5v1 height to run the aeroelastic study. The sketch of the blade surface, presented in Figure 2, shows thin, highly staggered blades with low camber, which is typical of transonic fan tip airfoils.

Choke flutter is associated with negative incidence and strong shock-wave choking the interblade channel. It appears for part-speed regime, typically around 80% of the nominal rotational speed. For the aeroelastic study, the operating point showing the highest massflow on 80Nn speed characteristic line is thus chosen (see Figure 1).

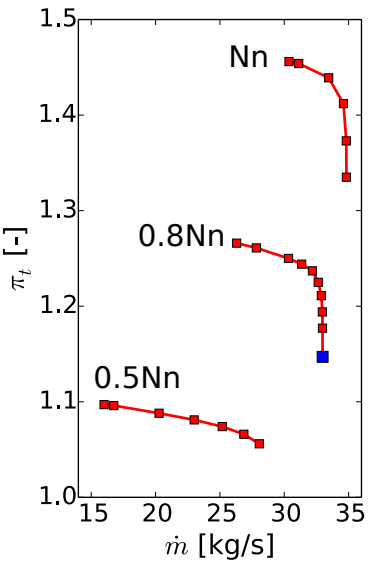

Figure 1: Operating range of ECL5v1 - choked operating point in blue

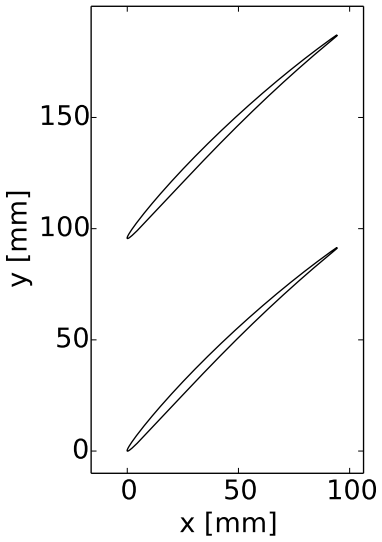

Figure 2: Sketch of aerodynamic airfoils at 90% height

3.2 Steady flow

The mesh used for both steady and unsteady computations has been obtain through a convergence study. It consists in 106,007 points with $y^+ < 1$ for the first layer of cells close to the blade surface. Total pressure, total temperature and azimuthal velocity are imposed at the upstream boundary and the static pressure at downstream boundary.

The steady relative Mach number associated to the choked flow is plotted in Figure 3. Looking at the leading edge zone, negative incidence can be seen as well as a supersonic region choking the interblade channel and terminated by a strong shock-wave. On the pressure side, the maximal Mach number is 1.23 and the boundary layer is attached to the blade downstream of the shock-wave. On the suction side, the Mach number reaches 1.32 which leads to the separation of the boundary layer downstream of the shock-wave. The separation is closed and the reattachment point is located 8.3% of chord downstream of the separation point.

3.3 Modeshape

Transonic flutter generally occurs along the first 3D bending mode of the blade. In a 2D blade to blade reference plane, this corresponds to a rigid body motion, *i.e.* without deformation of the blade surface. In this study, the chosen modeshape consists in a rotation of the airfoil around its leading edge. Three different positions of the blade during a vibration cycle are plotted in Figure 4.

In turbomachinery aeroelaticity, the motion of adjacent blades is coupled. For tuned blades, the frequency and modeshape are identical but a phase shift exists between two adjacent blades, called interblade phase angle or IBPA. Because of the annular periodicity of the rotor, the IBPA can only reach discrete values. In the reference frame of the rotor, it can be seen as a circumferential travelling wave. The IBPA is by convention positive when the wave propagates in the same direction than the rotor speed and negative otherwise.

Flutter usually appears for positive IBPA lower than 90°. In this work, the two extremes IBPA

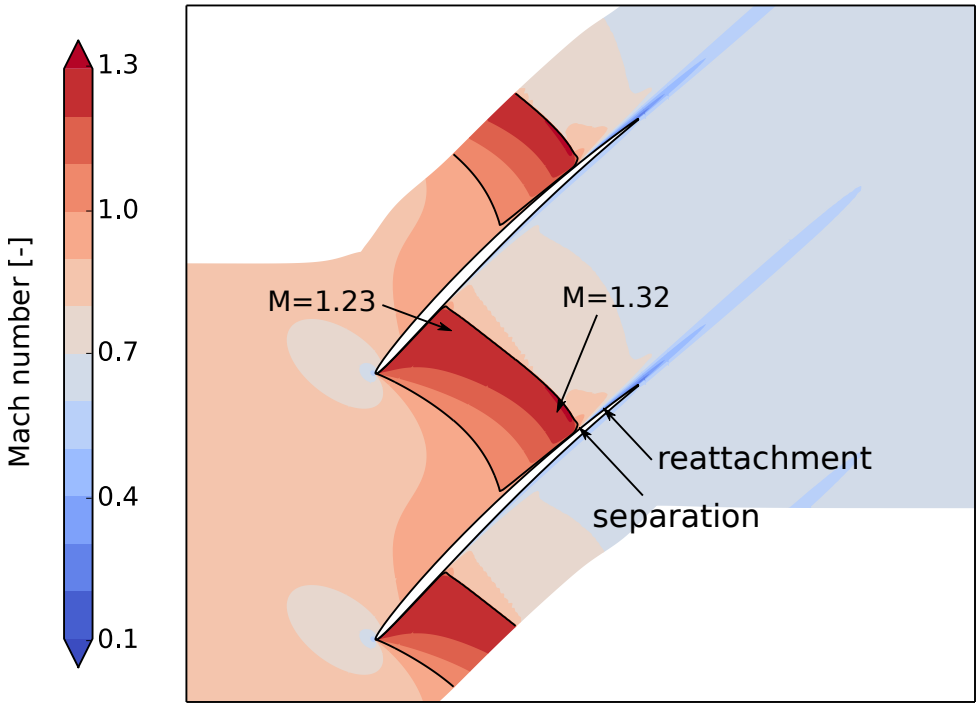

Figure 3: Steady relative Mach number for choked flow

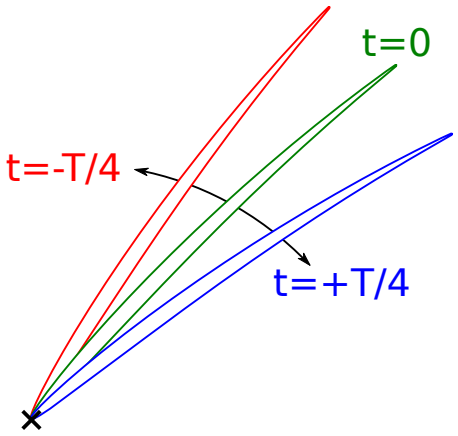

Figure 4: Sketch of three blade positions during a vibration cycle - rotation around leading edge

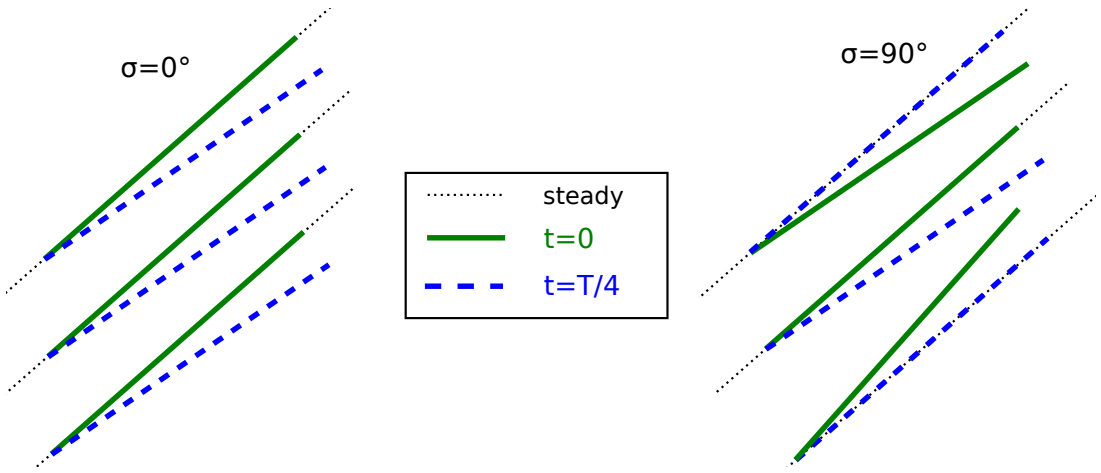

Figure 5: Sketch of blades position during a vibration cycle for $\sigma = 0^\circ$ and $\sigma = 90^\circ$ (steady blade position in black dashed lines)

0°and 90°are investigated. A sketch of the blades position during the vibration cycle for these two phase shifts is plotted in Figure 5. It can be seen for $\sigma = 90^\circ$ that the adjacent blades motion are out of phase. This leads to a maximal area fluctuation which in turn leads to strong velocity fluctuations.

The geometry, steady flow and modeshape presented here are used in the next section for the aeroelastic study. An innovative methodology is also presented to investigate the physical mechanisms leading to choke flutter.

4 AEROELASTIC STUDY

4.1 Influence of interblade phase angle (IBPA)

The influence of IBPA on aeroelastic stability is first investigated. The reduced frequency of the vibration based on the blade chord is $k = 0.15$. At this low frequency, the unsteady flow around the blade can be considered quasi-steady.

The real part of pressure fluctuations for $\sigma = 0^\circ$ is plotted on the left in Figure 6. The largest fluctuations can be seen around the steady position of the shock-wave (dashed black line) as well as in shock-wave / boundary layer interaction regions. The pressure fluctuations associated to the shock-wave motion at the center of interblade channel and close to the wall are out of phase. This may indicate a high contribution of viscous effects in shock-wave / boundary layer interaction regions. It can also be observed that pressure fluctuations almost vanish upstream and downstream of the shock-wave.

The real part of pressure fluctuations for $\sigma = 90^\circ$ is plotted on the right in Figure 6. The fluctuations levels are larger than those observed for $\sigma = 0^\circ$ in every part of the flow. This is a direct consequence of the large velocity fluctuations induced by the area variations for $\sigma = 90^\circ$. Locally, the stronger fluctuations occur near the steady shock-wave position and in shock-wave / boundary layer interaction regions. For this IBPA, large fluctuations are also observed upstream of the blades and in the interblade channel downstream of the shock-wave.

To analyse the aeroelastic stability, the extracted work is plotted along blade chord in Figure 7 for both IBPA ($\sigma = 0^\circ$ and $\sigma = 90^\circ$). Leading edge is at $x/c = 0$, negative abscissa corresponds to the pressure side and positive abscissa to the suction side. Upstream of the steady

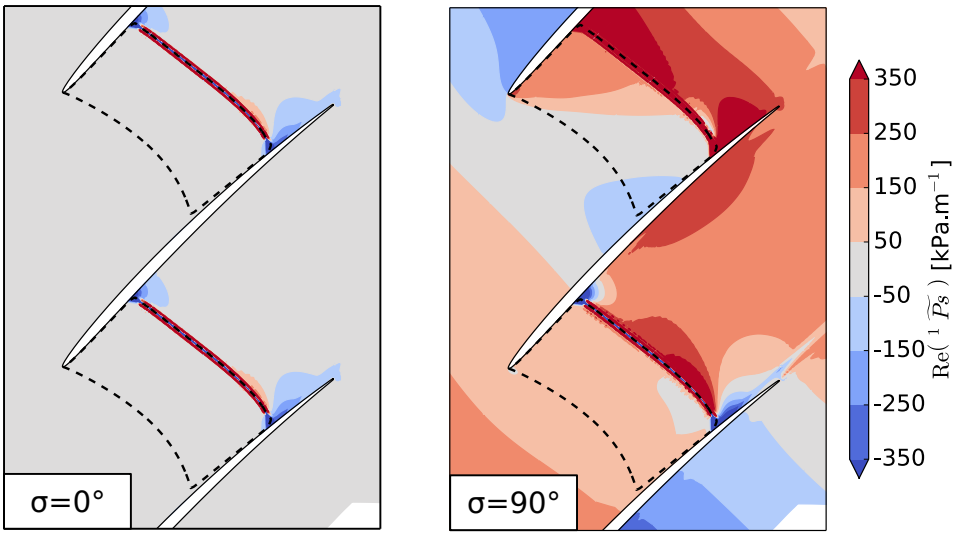

Figure 6: Real part of pressure fluctuations for $\sigma = 0^\circ$ (left) and $\sigma = 90^\circ$ (right) - $k = 0.15$

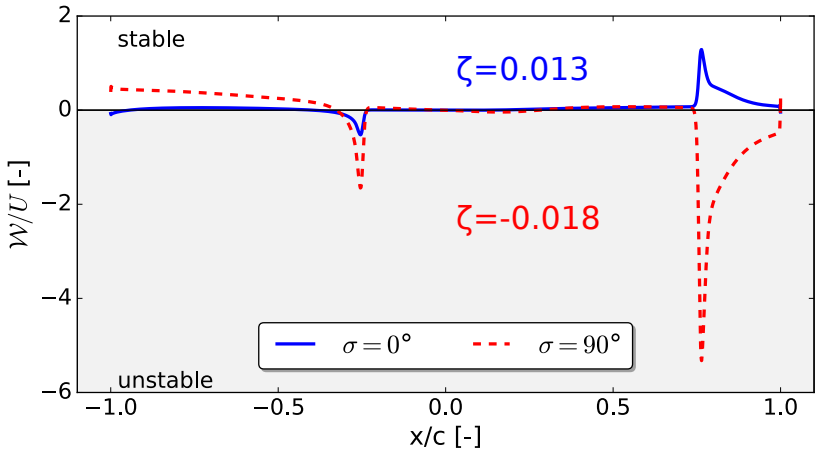

Figure 7: Extracted work along blade chord for $\sigma = 0^\circ$ and $\sigma = 90^\circ$ (leading edge at $x/c = 0$, pressure side: $x/c < 0$, suction side: $x/c > 0$) - $k = 0.15$

shock-wave ($-0.25 < x/c < 0.75$), the extracted work is very low for both IBPA which corresponds to a neutral contribution to stability (neither stabilising nor destabilising). On the pressure side, the shock-wave shows a destabilising contribution ($x/c = -0.25$) for both IBPA. This contribution is larger for $\sigma = 90^\circ$ because of larger pressure fluctuations (see Figure 6). Downstream of the steady shock-wave ($-1.0 < x/c < -0.25$), a neutral contribution is observed for $\sigma = 0^\circ$ while it is stabilising for $\sigma = 90^\circ$.

On the suction side, the contribution of the shock-wave motion is opposite for the two IBPA. For $\sigma = 0^\circ$, the contribution is stabilising and 2.5 times larger than the pressure side shock-wave contribution. For $\sigma = 0^\circ$, the contribution is destabilising and 3.3 times larger than the pressure side shock-wave contribution. In both case, the separated boundary layer ($x/c > 0.8$) shows an important contribution (same sign than the shock-wave contribution). The damping coefficient is computed through the integral of the extracted work along the chord (see Equation (3)). For $\sigma = 0^\circ$, the damping coefficient is positive ($\zeta = 0.013$) which corresponds to a stable configuration. However, for $\sigma = 90^\circ$, the damping coefficient is negative ($\zeta = -0.018$). This means that an aeroelatic instability (choke flutter) occurs at reduced frequency $k = 0.15$ for the IBPA $\sigma = 90^\circ$.

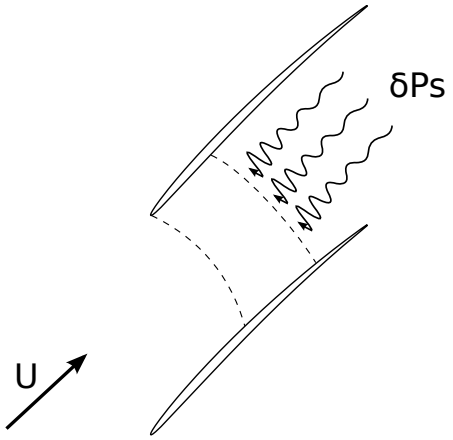

Figure 8: Acoustic blocage: wavelength decreasing and amplitude increasing of backward travelling pressure waves when approaching the shock-wave

4.2 Identifying flutter source

In the previous section, a choke flutter event has been encountered at $k = 0.15$ and $\sigma = 90^\circ$. In this section, the mechanisms leading to such an instability are identified thanks to an innovative methodology relying on the linearisation of RANS equation. Recall from Section 2.3 that the blade motion is modelled by imposing displacement and velocity on each node of the blade surface mesh. According to superposition principle, the unsteady flow generated by the vibration of the whole blade is equal to the sum of unsteady flows generated by the vibration of each surface mesh node. The blade motion can thus be decomposed in an arbitrary number of zones N and the global damping coefficient can be computed by the sum of the damping coefficient associated to each motion. Formally,

$$\zeta = \sum_{i}^{N} \zeta_i \quad ; \quad \zeta_i = \frac{1}{4\pi \mathcal{U}} \iint_{\Omega} \Re(\,{}^1\widetilde{Ps_i})\, \mathbf{S} \cdot \Re(\,{}^1\widetilde{\mathbf{V}}) \mathrm{d}\Omega \tag{6}$$

where $\widetilde{Ps_i}$ represents the pressure fluctuations generated by the motion of zone i. The definition of each zone should rely on physical insights.

For choke flutter, previous studies have shown the important contribution of backward travelling pressure waves [16, 17]. Such waves are generated downstream of the shock-wave and propagate upstream with a velocity $c - U$ where U is the velocity of the steady flow and c the sound celerity. When reaching the shock-wave, the velocity of backward travelling pressure waves decreases which leads to an increasing of their amplitude. This phenomenon, known as acoustic blocage, has been described by Atassi et al. [18] and is sketched in Figure 8.

To identify the contribution of acoustic blocage to the overall aeroelastic response, the blade is cut into $N = 2$ different regions represented in Figure 9. The upstream region (in blue) extends form the leading edge to the shock-wave / boundary layer interaction region while the downstream region (in red) corresponds to the remaining part of the blade. With such a decomposition, the only downstream contribution to the shock-wave motion is achieved through acoustic blocage. On the other hand, the vibration of the upstream part contributes through pressure waves (mainly generated at leading edge) and the local excitation of the shock-wave and the separated boundary layer on the suction side. It has been verified that the sum of these two contributions is equal to the aeroelastic response when the entire blade vibrates.

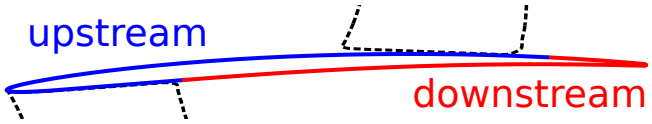

Figure 9: Blade surface decomposition in a downstream region (in red) and an upstream one (in blue)

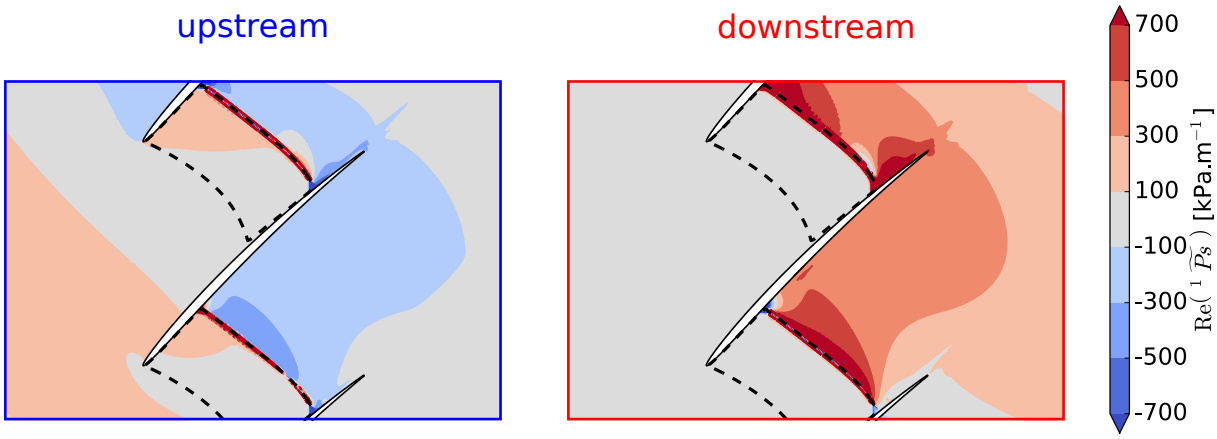

Figure 10: Real part of pressure fluctuations for upstream vibration (left) and downstream vibration (right) - $\sigma = 90^\circ$, $k = 0.15$

The real part of pressure fluctuations associated to the upstream and downstream vibration is plotted in Figure 10. Looking at the upstream contribution (left), fluctuations occur in the interblade channel as well as upstream and downstream of the blade row. The fluctuations are larger in the vicinity of the steady shock-wave than in any other part of the flow. Concerning the downstream contribution (right in Figure 10), the fluctuations produced downstream of the shock-wave cannot travel through the supersonic zone. Indeed, no fluctuations are observed upstream of the shock-wave. In the downstream part of the flow, the largest fluctuations are seen in the vicinity of the steady shock-wave as well as in the sock-wave / boundary layer interaction region which indicates a high contribution of viscous effects.

To analyse the contribution of upstream and downstream motion to the stability, the extracted work is plotted for each contribution in Figure 11. Once again, the shock-waves are responsible for the largest part of the overall stability. For the upstream vibration, the shock-wave has a stabilising effect on both sides of the blade, the largest contribution being achieved on the suction side where the boundary layer is separated. A noticeable destabilising contribution of the pressure side can also be seen downstream of the shock-wave. The aeroelastic response of the blade to the upstream vibration is stable ($\zeta = 0.010$). On the other hand, shock-wave has a destabilising effect for the downstream vibration on both sides. Once again, the destabilising contribution is larger on the suction side than on the pressure side. On the pressure side, a stabilising contribution is observed downstream of the shock-wave. The aeroelastic response of the blade to the downstream vibration is unstable ($\zeta = -0.028$). The upstream and downstream vibration contribute oppositely to the overall stability. Recall that the pressure fluctuations are higher for the downstream vibration because of acoustic blocage. Thus the aeroelastic behaviour of the blade is mainly driven by the downstream vibration.

Finally, it has been shown that the vibration of the downstream part of the blade drives the aeroelastic response. This confirms the important role of acoustic blocage in choke flutter instability. To further analyse the contribution of the backward travelling pressure wave, the influence of

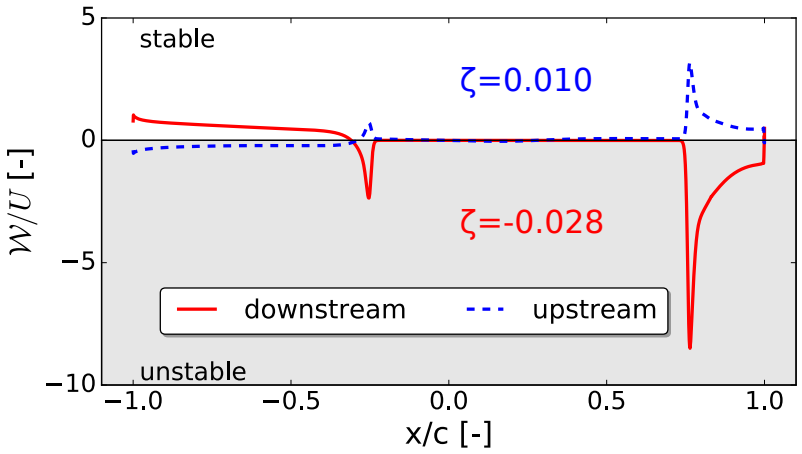

Figure 11: Extracted work along blade chord for upstream and downstream vibration - $\sigma = 90^\circ$, $k = 0.15$ (leading edge at $x/c = 0$, pressure side: $x/c < 0$, suction side: $x/c > 0$)

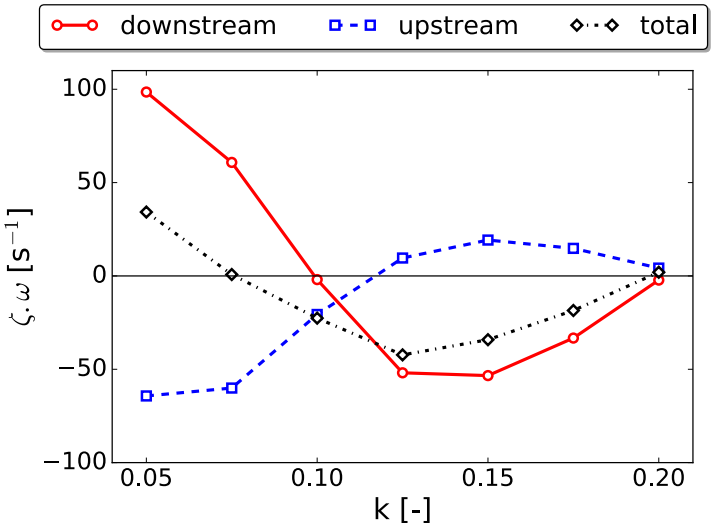

Figure 12: Normalised power associated to the upstream (in blue), downstream (in red) and total (black) vibration of the blade - $\sigma = 90^\circ$

reduced frequency is investigated in the next section.

4.3 Stability sensitivity to reduced frequency

The influence of reduced frequency on upstream and downstream vibration contribution to overall stability is now investigated for the IBPA $\sigma = 90^\circ$. The frequencies studied range from $k = 0.05$ to $k = 0.2$. For each frequency, two linear computations are run (one for the upstream vibration and one for the downstream vibration). The damping coefficient associated to each vibration is then computed. The product of damping coefficient by the pulse (normalised power) is plotted in Figure 12. This product represents the energy exchanged during a given time rather than during a vibration cycle.

The contribution of the downstream vibration is highly stabilising at low reduced frequency ($k = 0.05$). It then decreases, reaching a neutral contribution at $k = 0.10$ and a minimum at $k = 0.15$ where choke flutter has been encountered. The damping coefficient then rises and reach a neutral contribution at $k = 0.20$. The contribution of the upstream vibration behaves oppositely.

It is indeed destabilising at low reduced frequency ($k = 0.05$) and increases until reaching a maximum at $k = 0.15$. It then decreases until reaching a neutral contribution at $k = 0.20$. Regarding the absolute value of the damping coefficient associated to each contribution, it can be seen that the downstream is larger for the whole range of frequencies. This is a consequence of the acoustic blocage which amplifies the backward pressure waves generated downstream of the shock-wave. As a result, the trend of the total damping coefficient is quite similar to the trend of the downstream contribution. This global analysis shows that the aeroelastic behaviour of the blade is driven by its downstream contribution independently of the reduced frequency.

4.4 Influence of reduced frequency on downstream contribution

It has been showed that the aeroelastic instability is driven by the downstream vibration of the blade through acoustic blocage. This last section thus investigates the influence of reduced frequency on the downstream contribution.

Recall that the damping coefficient is a global parameter computed through the integral of the extracted work along the entire blade (see Equation (3)). This parameter is plotted in Figure 12 and Figure 13 in solid red line. To anayse the contribution of the shock-wave, the integral in Equation (3) can be bounded to the shock-wave / boundary layer interaction (SWBLI) regions on the suction side (blue dashed line in Figure 13) and the pressure side (green dashed line in Figure 13). Compared to the entire blade, the sum of the SWBLI contributions (red dashed line in Figure 13) has a similar trend but lower values. Outside the SWBLI regions, the contribution is thus positive and approximately constant with respect to the reduced frequency. This emphasises the destabilising influence of the shock-wave motion. Looking more closely, the SWBLI pressure side contribution is stabilising at low reduced frequency ($k = 0.05$) and decreases until reaching a slightly destabilising contribution at $k = 0.20$. The average damping coefficient on the range $0.05 < k < 0.20$ is small yet positive. On the other hand, the suction side contribution is always destabilising and non monotonic, reaching a maximal negative contribution at $k = 0.125$. Its average damping coefficient on the range $0.05 < k < 0.20$ is negative and significant. The SWBLI thus behaves differently on the pressure side and the suction side, the latter giving the largest contribution. Recall that the work extracted depends on the blade velocity which is higher at the SWBLI region on the suction side that on the pressure side (the shock-wave being located further from the rotation center, see Figure 4). Moreover, viscous effects associated to the separated boundary layer can also lead to higher pressure fluctuations.

To analyse the local unsteady flow, the real part of pressure fluctuations is plotted in Figure 14. At low reduced frequency $k = 0.05$, the pressure fluctuations in the SWBLI region are weaker on the suction side than on the pressure side. For the suction side, even if the velocity is stronger, this leads to a smaller absolute value of damping coefficient (see Figure 14, $k = 0.05$). As the reduced frequency increases to $k = 0.10$, the pressure fluctuations increase in the SWBLI region on the suction side (green arrow), leading to a larger destabilising contribution. The magnitude of pressure fluctuations is now comparable between the pressure side and the suction side SWBLI region. From $k = 0.10$ to $k = 0.15$, the SWBLI contribution switches from stabilising to destabilising on the pressure side (magenta arrow). At the same time, the SWBLI zone becomes sharper on the pressure side while it is still wide on the suction side. From $k = 0.15$ to $k = 0.20$, the pressure fluctuations on the suction side decrease and almost vanish in the SWBLI region (blue arrow). The pressure side does not exhibit any change in the SWBLI region while the pressure fluctuations are lower behind it.

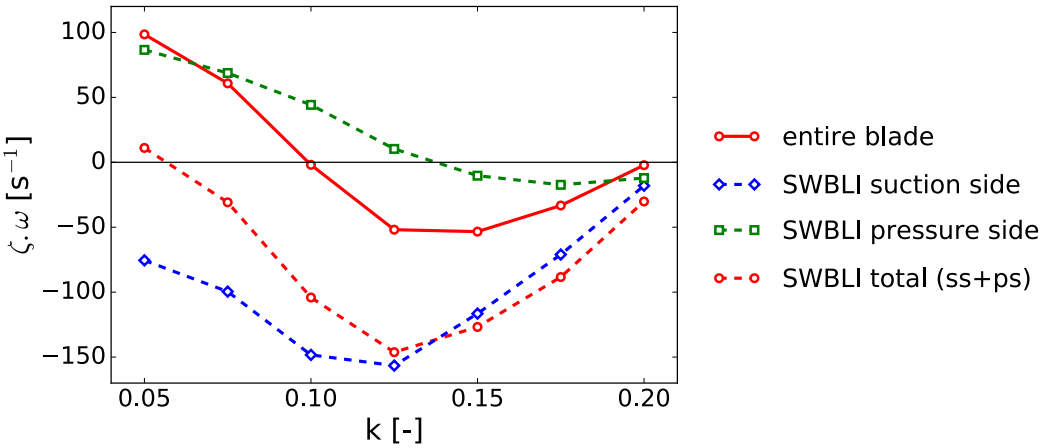

Figure 13: Normalised power associated to the downstream vibration extracted along the entire blade (solid line) or only in shock-wave / boundary layer interaction regions (SWBLI, dashed lines) - $\sigma = 90^\circ$

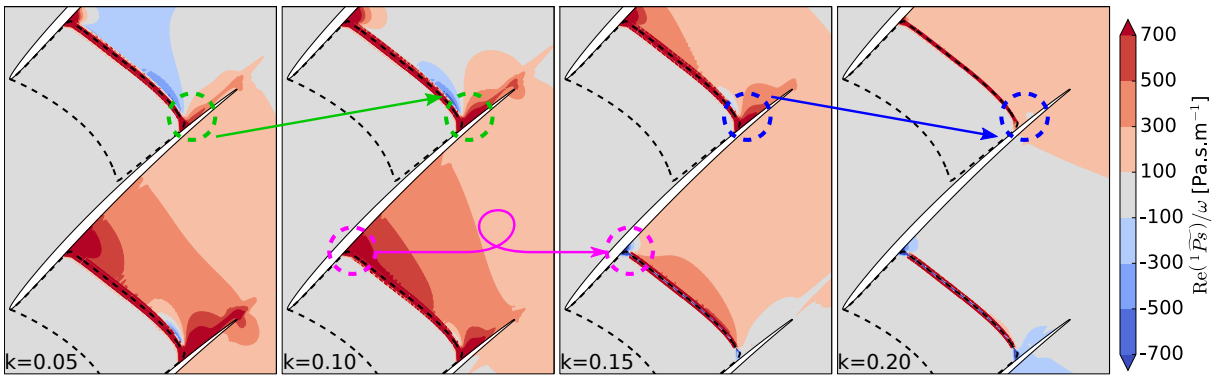

Figure 14: Real part of pressure fluctuations associated to the downstream vibration for different reduced frequencies at $\sigma = 90^\circ$ - in SWBLI regions : increase of pressure fluctuations in green, decrease in blue, inversion of the stability in magenta

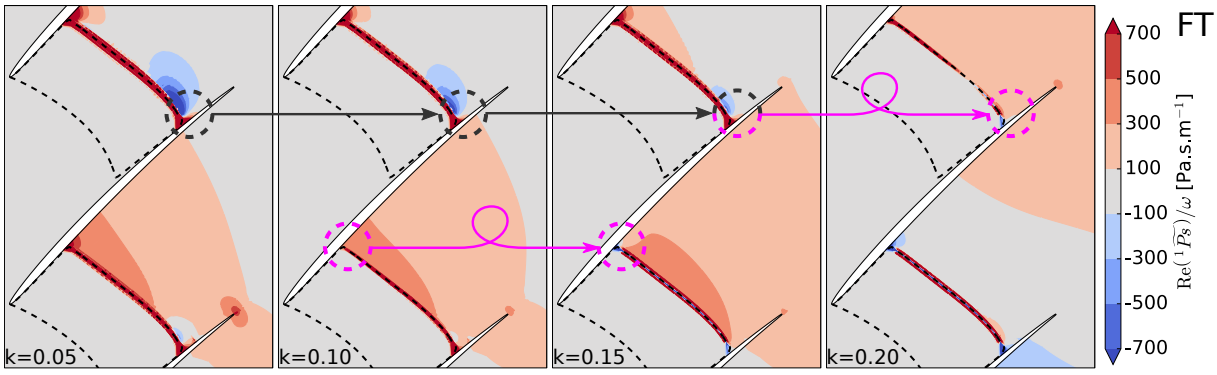

Figure 15: Real part of pressure fluctuations associated to the downstream vibration with constant turbulent viscosity (FT : frozen turbulence) for different reduced frequencies at $\sigma = 90^\circ$ - in SWBLI regions : stagnation of pressure fluctuations in grey, inversion of the stability in magenta

Differences have been observed between the unsteady behaviour of the SWBLI on the pressure and suction side. In the steady flow, the main difference between the pressure and suction side SWBLI is the separated boundary layer on the latter. The unsteady viscous effects associated to the separation could explain the differences aforementioned. To evaluate this hypothesis, frozen turbulence computations (*i.e.* with constant turbulent viscosity) have been run. The real part of the pressure fluctuations with constant turbulent viscosity is plotted in Figure 15. First, it can be observed that the SWBLI zones are very sharp with much lower magnitude of pressure fluctuations. This indicates a significant influence of unsteady viscous effects, particularly at low frequencies ($k \leq 0.10$) for which the differences are the largest. In the suction side SWBLI region, the pressure fluctuations do not vary from $k = 0.05$ to $k = 0.15$ (grey arrow) and then switches from a destabilising to a stabilising contribution between $k = 0.15$ and $k = 0.20$ (magenta arrow). On the pressure side, the SWBLI contribution is destabilising at high frequencies ($k \geq 0.15$) and very similar to the behaviour observed in Figure 14. The low frequencies ($k \leq 0.10$) are again associated to a stabilising contribution of the SWBLI. These results show that viscous effects influence the magnitude of the extracted work in weak SWBLI (on the pressure side) whereas it impacts both magnitude and sign in strong SWBLI (on the suction side).

The aeroelastic study presented here showed an event of choke flutter at a reduced frequency $k = 0.15$ and an interblade phase angle $\sigma = 90^\circ$. An innovative methodology relying on linear decomposition has been used to identify the downstream vibration of the blade as the main mechanism leading to choke flutter. Through further analysis, the phenomenon of acoustic blocage could be associated to the downstream vibration, leading to large pressure fluctuations in the vicinity of the steady shock-wave position. This mechanisms being independent of the frequency, the downstream vibration drives the blade stability for the whole range of studied frequencies. Through a local analysis, the destabilising contribution of the downstream vibration has been associated with the behaviour of the unsteady shock-wave / separated boundary layer interaction on the suction side. Finally, it has been shown that both amplitude and phase of pressure fluctuations depend on unsteady viscous effects in strong SWBLI.

5 CONCLUSION

This work aimed at a better understanding of physical mechanisms responsible for choke flutter in UHBR transonic fan. The current design of the transonic research fan ECL5 has been used to support this study. A blade to blade channel at 90% height has been chosen for the 2D aeroelastic analysis. The modeshape consists in a rigid body motion rotation around the leading edge with $\sigma = 0^\circ$ and $\sigma = 90^\circ$ interblade phase angles. State of the art nonlinear and linear RANS solvers were used to compute the steady flow and the linearised unsteady flow around the blades. A choke flutter event has been observed at reduced frequency $k = 0.15$ and for the interblade phase angle $\sigma = 90^\circ$.

As a main contribution of this work, an innovative methodology has been proposed to identify the source of the instability. This methodology relies on linear computations to decompose the blade motion into two parts. It has been successfully applied and showed that the aeroelastic behaviour of the blade is driven by the vibration of the profile downstream of the shock-wave through the phenomenon of acoustic blocage.

Another contribution is the local analysis of the unsteady flow associated to the downstream vibration. Computing the damping coefficient for different zones, the largest contribution to

stability has been associated to the unsteady shock-wave / separated boundary layer interaction on the suction side. The analysis of the pressure fluctuations in the interblade channel for different frequencies finally showed the major contribution of the unsteady viscous effects on the choke flutter instability.

The results on the importance of acoustic blocage open an interesting perspective for the design of choke flutter active control device. Piezoelectric actuators located near the rotor blade trailing edge or at the leading edge of the following stator blades can efficiently triggers or damps choke flutter in experimental facilities dedicated to aeroelastic studies.

The large contribution of unsteady viscous effects highlights the increasing need for local unsteady experimental data and may lead to new aeroelastic control concepts through the control of the separated boundary layer.

Finally, the linear decomposition method presented here is not limited to turbomachinery aeroelasticity and should be used whenever a deeper understanding of the unsteady flow is needed. The decomposition strategy should be adapted for each application. Even for unsteady flows, one can evaluate the remaining coupling terms by withdrawing the linear response associated to each perturbation.

6 REFERENCES

[1] Micklow, J. and Jeffers, J. (1981). Semi-actuator disk theory for compressor choke flutter. Tech. Rep. 19810016540, NASA.

[2] Dowell, E., Clark, R., Cox, D., et al. (2004). *A modern course in aeroelasticity*, vol. 3. Springer.

[3] Jutras, R., Stallone, M., and Bankhead, H. (1981). Experimental investigation of flutter in midstage compressor designs. *Journal of Aircraft*, 18(10), 874–880.

[4] Marshall, J. and Imregun, M. (1996). A review of aeroelasticity methods with emphasis on turbomachinery applications. *Journal of Fluids and Structure*, 10.

[5] Petrie-Repar, P. J., McGhee, A., Jacobs, P. A., et al. (2006). Analytical maps of aerodynamic damping as a function of operating condition for a compressor profile. In *ASME Turbo Expo 2006: Power for Land, Sea, and Air*. American Society of Mechanical Engineers, pp. 1133–1144.

[6] Smati, L., Aubert, S., Ferrand, P., et al. (1997). Comparison of numerical schemes to investigate blade flutter. *Proceedings of the 8th International Symposium of Unsteady Aerodynamics, Aeroacoustics and Aeroelasticity of Turbomachines*.

[7] Roe, P. (1981). Approximate riemann solvers, parameter vectors, and difference schemes. *Journal of computational physics*, 43(2), 357–372.

[8] Van Leer, B. (1979). Towards the ultimate conservative difference scheme. v. a second-order sequel to godunov's method. *Journal of computational Physics*, 32(1), 101–136.

[9] Saad, Y. and Schultz, M. (1986). GMRES : a generalized minimal residual algorithm for solving nonsymmetric linear systems. *SIAM Journal on Scientific and Statistical Computing*, 7(3).

[10] Wilcox, D. C. (1988). Reassessment of the scale determining equation for advanced turbulence models. *AIAA Journal*, 26(11).

[11] Philit, M., Ferrand, P., Labit, S., et al. (2012). Derivated turbulence model to predict harmonic loads in transonic separated flows over a bump. In *28th International Congress of Aeronautical Sciences*.

[12] Rendu, Q., Philit, M., Labit, S., et al. (2015). Time-linearized and harmonic balance Navier-Stokes computations of a transonic flow over an oscillating bump. In *11th International Symposium on Unsteady Aerodynamics, Aeroacoustics & Aeroelasticity of Turbomachines*. Stockholm, Sweden.

[13] Jameson, A., Schmidt, W., and Turkel, E. (1981). Numerical solution of the euler equations by finite volume methods using runge-kutta time-stepping schemes. In *14th AIAA Fluid and Plasma Dynamic Conference*. Palo Alto, CA.

[14] Verdon, J. (1987). Linearized unsteady aerodynamic theory. In *AGARD Manual : Aeroelasticity in axial-flow turbomachines vol.1*. Platzer, M.F. & Carta, F.O.

[15] Rendu, Q. (2016). *Modélisation des écoulements transsoniques décollés pour l'étude des interactions fluide-structure*. Ph.D. thesis, Université de Lyon.

[16] Ferrand, P. (1987). Parametric study of choke flutter with a linear theory. In *Advanced technology for aero gas turbine components*. AGARD CP 421.

[17] Rendu, Q., Rozenberg, Y., Aubert, S., et al. (2016). Investigation of shock-wave/boundary-layer interaction on aeroelastic stability : towards active control. In *ASME Paper GT2016-57302*. Seoul, South Korea.

[18] Atassi, H., Fang, J., and Ferrand, P. (1995). Acoustic blockage effects in unsteady transonic nozzle and cascade flows. In *33rd AIAA Aerospace Sciences Meeting*. Reno, NV.

COPYRIGHT STATEMENT